Journal of Electron Spectroscopy and Related Phenomena 209 (2016) 1–8

Contents lists available at ScienceDirect

Journal of Electron Spectroscopy and Related Phenomena

journal homepage: www.elsevier.com/locate/elspec

Quantitative study of the *f* occupation in Ce*M*In$_5$ and other cerium compounds with hard X-rays

M. Sundermann[a,*], F. Strigari[a], T. Willers[a], J. Weinen[b], Y.F. Liao[c], K.-D. Tsuei[c], N. Hiraoka[c], H. Ishii[c], H. Yamaoka[d], J. Mizuki[f,e], Y. Zekko[f], E.D. Bauer[g], J.L. Sarrao[g], J.D. Thompson[g], P. Lejay[h], Y. Muro[i], K. Yutani[j], T. Takabatake[j,k], A. Tanaka[j], N. Hollmann[b], L.H. Tjeng[b], A. Severing[a,**]

[a] *Institute of Physics II, University of Cologne, Zülpicher Straße 77, 50937 Cologne, Germany*
[b] *Max Planck Institute for Chemical Physics of Solids, Nöthnizer Straße 40, 01187 Dresden, Germany*
[c] *National Synchrotron Radiation Research Center, 101 Hsin-Ann Road, Hsinchu 30077, Taiwan*
[d] *RIKEN SPring-8 Center, 1-1-1 Kouto, Sayo, Hyogo 679-5148, Japan*
[e] *Japan Atomic Energy Agency, SPring-8, 1-1-1 Kouto, Mikazuki, Sayo, Hyogo 679-5148, Japan*
[f] *Graduate School of Science and Technology, Kwansei Gakuin University, Sanda, Hyogo 669-1337, Japan*
[g] *Los Alamos National Laboratory, Los Alamos, NM 87545, USA*
[h] *Institut NEEL, CNRS, 25 rue des Martyrs, 38042 Grenoble cedex 9, France*
[i] *Faculty of Engineering, Toyama Prefectural University, Izumi 939-0398, Japan*
[j] *Department of Quantum Matter, AdSM, Hiroshima University, Higashi-Hiroshima 739-8530, Japan*
[k] *Institute for Advanced Materials Research, Hiroshima University, Higashi-Hiroshima 739-8530, Japan*

ARTICLE INFO

Article history:
Received 8 December 2015
Received in revised form 16 February 2016
Accepted 19 February 2016
Available online 28 February 2016

Keywords:
Heavy fermion
Valence
Hard X-ray photoelectron spectroscopy
L-edge X-ray absorption
Full multiplet
Single impurity Anderson model

ABSTRACT

We present bulk-sensitive hard X-ray photoelectron spectroscopy (HAXPES) data of the Ce3*d* core levels and lifetime-reduced *L*-edge X-ray absorption spectroscopy (XAS) in the partial fluorescence yield (PFY) mode of the Ce*M*In$_5$ family with M = Co, Rh, and Ir. The HAXPES data are analyzed quantitatively with a combination of full multiplet and configuration interaction model which allows correcting for the strong plasmons in the Ce*M*In$_5$ HAXPES data, and reliable weights w_n of the different f^n contributions in the ground state are determined. The Ce*M*In$_5$ results are compared to HAXPES data of other heavy fermion compounds and a systematic decrease of the hybridization strength V_{eff} from $CePd_3$ to $CeRh_3B_2$ to $CeRu_2Si_2$ is observed, while it is smallest for the three Ce*M*In$_5$ compounds. The *f*-occupation, however, increases in the same sequence and is close to one for the Ce*M*In$_5$ family. The PFY-XAS data confirm an identical *f*-occupation in the three Ce*M*In$_5$ compounds and a phenomenological fit to these PFY-XAS data combined with a configuration interaction model yields consistent results.

1. Introduction

In intermetallic cerium compounds the hybridization of Ce *f* and conduction electrons (*cf*-hybridization) leads to two competing interactions: the Ruderman Kittel Yosida (RKKY) interaction prevailing for weak exchange interactions and favoring a magnetically ordered ground state and the Kondo screening which leads to a nonmagnetic ground state. Non-Fermi liquid behavior and unconventional superconductivity are often observed when going from the verge of one regime to the other. In the presence of strong *cf*-hybridization the *f*-electrons are even partially delocalized. The competition of both interactions can be influenced by pressure, magnetic field or substitution [1].

The Ce*M*In$_5$ compounds with M = Co, Rh and Ir are an interesting *model* system for investigating systematically why a compound orders magnetically or shows unconventional superconductivity because their phase diagram covers a variety of ground states: unconventional superconductivity (M = Co and Ir), antiferromagnetic order (M = Rh), and the coexistence of both e.g. when substituting on the transition metal site. There are also quantum critical points with Fermi surface changes when going from the more itinerant, superconducting Co-rich to the more localized, magnetically ordered Rh-rich side of the substitution phase diagram or when applying pressure to $CeRhIn_5$. It is believed that

* Corresponding author. Tel.: +49 351 4646 4323; fax: +49 351 4646 4902.
** Corresponding author. Tel.: +49 221 470 2608.
E-mail addresses: sundermann@ph2.uni-koeln.de (M. Sundermann), severing@ph2.uni-koeln.de (A. Severing).

http://dx.doi.org/10.1016/j.elspec.2016.02.002

stronger *cf*-hybridization favors the superconducting ground state over the magnetically ordered one [2–20]. It is therefore of interest to quantify the *cf*-hybridization. The 4*f*-shell occupation is often used as an indication for the degree of hybridization since strong hybridization favors the delocalization of *f* electrons. Here, we use a consistent analysis procedure that includes a quantitative plasmon correction to obtain the 4f occupation and that allows a meaningful comparison for materials with very different degrees of hybridization.

In the presence of strong *cf*-hybridization the cerium ground state is no longer a pure f^1 state with an *f*-electron count $n_f = 1$. Instead it can be written as a mixed state $|\Psi_{GS}\rangle = c_0\ |f^0\rangle + c_1\ |f^1\underline{L}\rangle + c_2\ |f^2\underline{\underline{L}}\rangle$ with additional contributions of the divalent and tetravalent states (f^2 and f^0) and a total *f* occupation n_f that can be related to the weights $w_n \equiv |c_n|^2$ ($n = 0,1,2$) of these ground states as $n_f = w_1 + 2w_2$. Here $\underline{L}$ and $\underline{\underline{L}}$ denote the conduction band with one and two holes, respectively. The amount of f^0 quantifies the degree of delocalization. Photoelectron spectroscopy (PES) and X-ray absorption (XAS) are invaluable in determining such mixed ground states since these – typically 3*d* core level PES and *L*-edge XAS – exhibit spectral weights at the energies of corel-electron removal states corresponding to three of these *f* states: $\underline{c}f^0$, $\underline{c}f^1\underline{L}$ and $\underline{c}f^2\underline{\underline{L}}$, where $\underline{c}$ represents a core hole. Although the intensities $I(\underline{c}f^0)$, $I(\underline{c}f^1\underline{L})$ and $I(\underline{c}f^2\underline{\underline{L}})$ (referred to as $I(f^0)$, $I(f^1)$ and $I(f^2)$ for simplicity) of these structures can be related to the weights of the *f* states w_0, w_1, and w_2 in the initial state, the relation is not simple because of the effects of the core-hole potential and hybridization in the final state [21–24]. The Anderson impurity model (AIM) in the formalism of Gunnarson and Schönhammer [22] has been a very successful analysis tool to relate final state spectral weights $I(f^n)$ to the respective *f* contributions w_n in the initial (ground) state. In Ref. [21] Fuggle et al. show and analyze an impressive amount of PES data of Ce compounds giving number for w_0 and hybridization parameters. However, PES data are often subject to surface effects and the surface valence is usually closer to integer than the one of the bulk [25]. Furthermore, the AIM in combination with a full multiplet routine would require elaborate computation so that usually the spectral weights are assigned phenomenologically. However, the spectral shapes (energy distribution) of the f^1 and f^2 contributions depend on the hybridization so that the assignment of spectral weights to $I(f^n)$ is not trivial, something desperately needed when aiming at a quantitative plasmon correction. The non-trivial assignment of spectral weights is also valid for *L*-edge XAS where the spectral shapes are determined by the empty 5*d* density-of-states (5*d*-DOS). This is valid even in the state-of-the-art partial fluorescent yield mode (PFY) which gives a much better contrast than conventional total fluorescence yield (TFY)-XAS [26–30]. It is therefore not trivial to find comparable numbers for the *f*-electron occupation.

There have been several attempts to determine the 4*f*-occupation of the Ce*M*In$_5$ family, however, quantitatively they are not conclusive [14,31–36]. XAS data at the Ce *M*-edge or resonant data at the *N*-edge of the Ce*M*In$_5$ compounds show only minor amounts of $I(f^0)$ without further quantification [14,32,34]. A more adventurous attempt to quantify the *f*-occupation of CeCoIn$_5$ and CeCo(In$_{0.85}$Cd$_{0.15}$)$_5$ in an *M*-edge XAS experiment was made by Howald et al. [37] from an extrapolation of CeF_3 and CeO_2 *M*-edge data, assuming the former is tri- and the latter tetravalent. However, there is a lot of work showing that CeO_2 appears strongly covalent ($n_f \approx 0.5$) in core-level spectroscopies like *L*- or *M*-edge XAS or PES (see e.g. Refs. [38–41] and references therein), thus putting into question the *f*-occupation of 0.85 resulting from this analysis. TFY-XAS data at the Ce *L*-edge yield $n_f = 0.9$ for CeCoIn$_5$ [35], and 0.98 and 0.96 for the Rh and Ir compounds, respectively [31]. In these TFY L_3-edge XAS data the $I(f^n)$ weights are not well resolved. The assignment is further complicated by the fine structure of the empty 5*d*-DOS and the multiple scattering features which in these compounds are close in energy to the main absorption line [31,35]. PES data at the Ce3*d* core level were taken with Al K_α radiation [33,36]. They bear the problem of surface sensitivity [25] and in addition exhibit strong plasmons at the energy of the $I(f^0)$ spectral weight. $n_f = 0.9$ was given as a lower limit for all three compounds without correcting quantitatively for the plasmons [36].

Here we present a quantitative analysis of bulk-sensitive HAXPES data of the Ce*M*In$_5$ family and compare data and analysis with the ones of the large T_K ($\approx$ 600 K) and intermediate valent compound $CePd_3$[42,43,21,44,23,45,46], intermediate valent and ferromagnetically ordered $CeRh_3B_2$ (T_c = 115 K) [47–49] and the heavy fermion compound $CeRu_2Si_2$, which does not order magnetically at ambient pressure and zero magnetic field [50,51].

Our HAXPES data analysis comprises a quantitative plasmon correction which we achieve by combining a full multiplet (fm) calculation with a configuration interaction (CI) model (fm-CI) with a single-state-approximation for the conduction band. It is a convenient simplification to determine the $I(f^n)$ spectral weights and relate them to w_n weights in the ground state. The model was already suggested by Imer and Wuilloud [52] and, although it has certain drawbacks [52,53], has the great advantage that it can be combined with a full multiplet calculation. This is particularly important for the Ce*M*In$_5$ compounds where strong plasmons would otherwise hamper the quantitative determination of spectral intensities [33,36]. The full multiplet calculation offers the possibility to describe the plasmon intensities as part of the line shape of each emission line, after having determined the plasmon parameters from core levels that are not affected by the configuration interaction (In3*p* for each Ce*M*In$_5$, Pd3*p* for $CePd_3$, Rh3*d* for $CeRh_3B_2$, and Ru3*d* for $CeRu_2Si_2$). We have used this type of analysis already successfully for the CeT_2Al$_{10}$ compounds [53] and we apply it here to obtain quantitative *f*-occupations for the Ce*M*In$_5$ compounds. The resulting values will be compared with the ones of $CePd_3$, $CeRh_3B_2$, and $CeRu_2Si_2$. The model is described by the CI parameters for the Coulomb exchange interaction between the *f* electrons (U_{ff}) and between the *f* electrons and 3*d* core hole (U_{fc}), the effective *f*-electron binding energy ε_f and the isotropic hybridization V_{eff}. The energy distances and intensities of the three $I(f^n)$ spectral weights in the 3*d* core level HAXPES data yield sufficient information for determining the four CI parameters in a unique manner.

We confirm our findings by showing *L*-edge absorption data in the PFY mode where a decay process with longer life time is selected so that the life time broadening of the XAS spectra can be reduced, thus facilitating the separation of the different $I(f^n)$ spectral weights [26–29]. Here we compare the Ce*M*In$_5$ spectra with the ones of the more strongly hybridized compounds Ce*T*Al$_{10}$[53] and present a fit to the data which is consistent with the HAXPES results.

The experimental set-ups of HAXPES and PFY-XAS including details for sample preparation are given in Appendix A and information of the data simulation and HAXPES line shapes are given in Appendix B.

2. Data and simulation

Fig. 1 shows the uncorrected 3*d* core level HAXPES data of Ce*M*In$_5$ (M = Ir, Rh, and Co), $CeRu_2Si_2$, $CeRh_3B_2$, and $CePd_3$. All spectra exhibit two sets of emission lines, due to the Ce3*d* spin orbit splitting. Each set, i.e. the Ce3$d_{3/2}$ and the Ce3$d_{5/2}$, contains three spectral weights because of the core hole effect on the mixed ground state. At the bottom of the $CePd_3$ data the energy positions of the two sets of $I(f^0)$, $I(f^1)$, and $I(f^2)$ are marked. It shows that the expected $I(f^0)$ spectral weight at 915 eV binding energy does

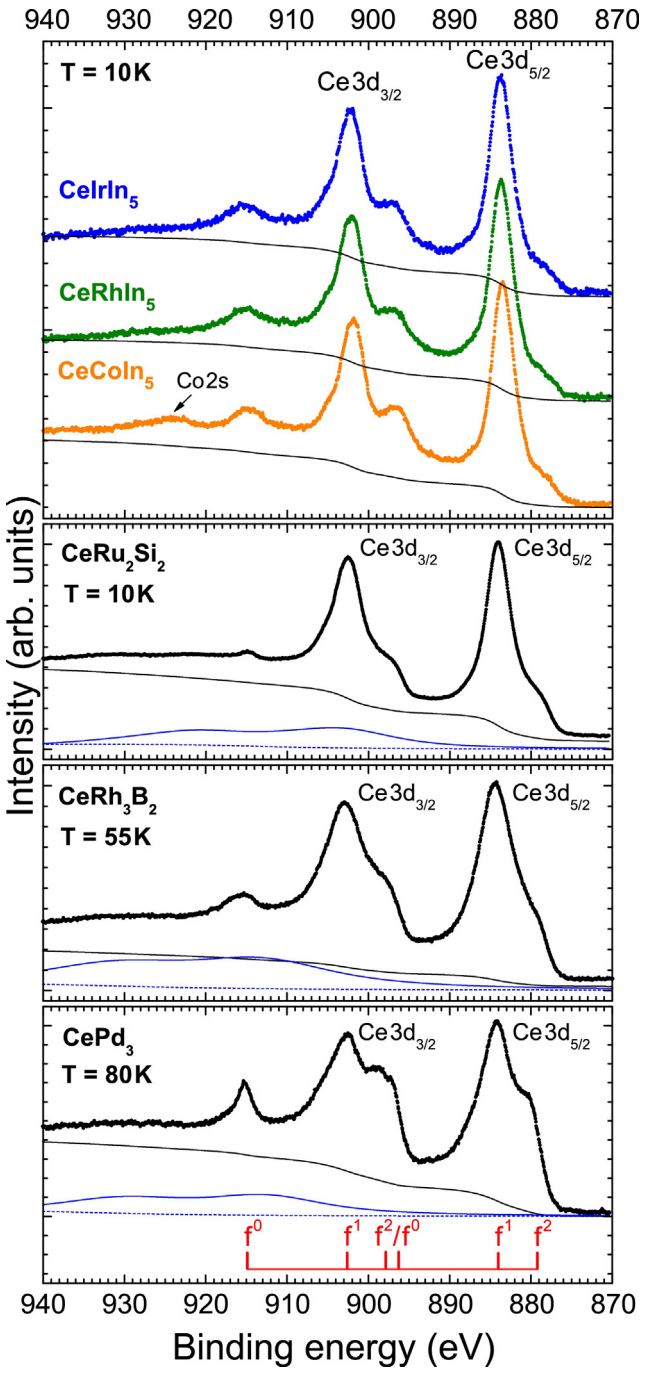

Fig. 1. Low temperature Ce3*d* HAXPES data as measured of Ce*M*In$_5$ (M = Ir, Rh, and Co), $CeRu_2Si_2$, $CeRh_3B_2$, and $CePd_3$. The solid black lines show the respective integral background. The solid and dashed blue lines show the 1st and 2nd plasmon contribution (see text). For the Ce*M*In$_5$ this is shown in Fig. 3. The red ruler in the bottom panel indicates the energy positions of the $I(f^n)$ spectral weights. (For interpretation of the references to color in this figure legend, the reader is referred to the web version of this article.)

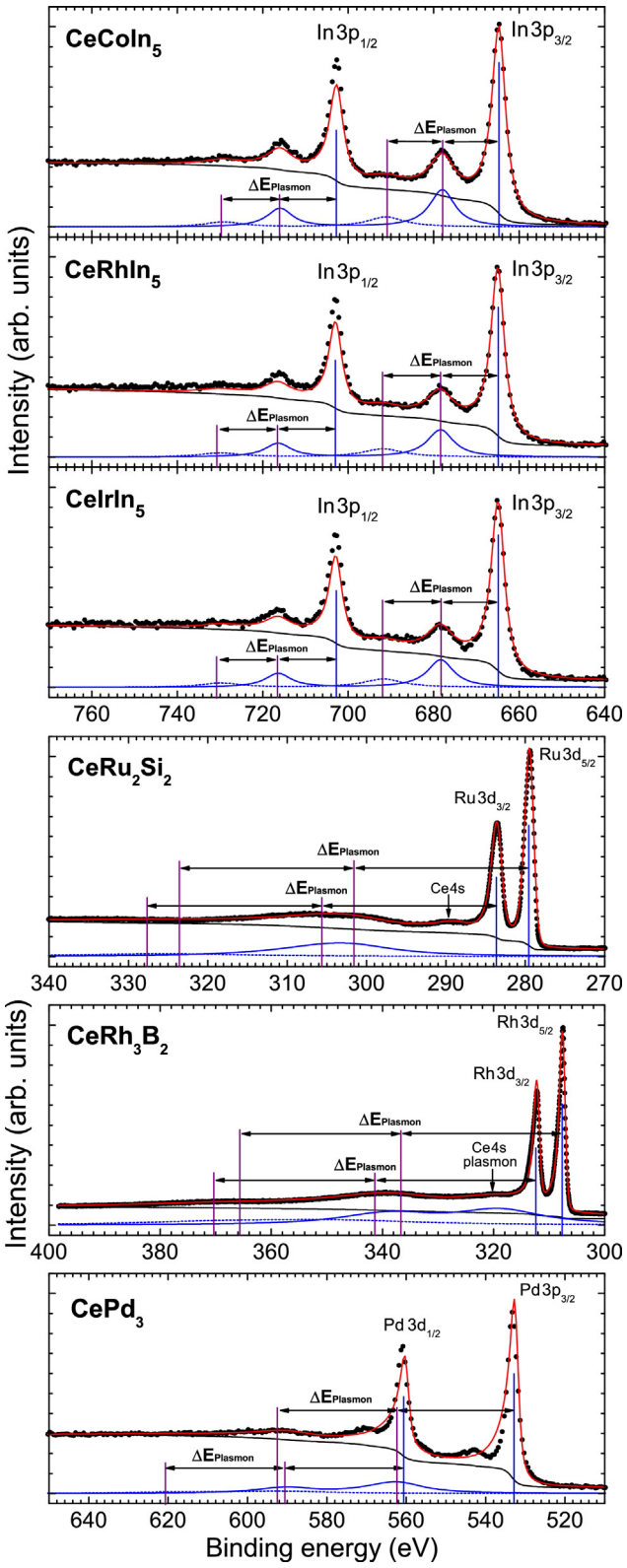

Fig. 2. Emission lines as measured of core levels that are not affected by the configuration interaction. The solid black lines are the integral background, the red lines are the result of an ionic calculation with adequate line shape parameters. The blue lines (solid and dashed) represent the total (1st and 2nd order) plasmon intensities which were obtained by fitting each emission line with a line shape consisting of the main emission line plus a 1st and 2nd plasmon contribution at equidistant energies. (For interpretation of the references to color in this figure legend, the reader is referred to the web version of this article.)

not overlap with any other spectral feature and that the $I(f^2)$ intensity at ≈880 eV overlaps only partially with $I(f^1)$. However, there is a multiplet structure underneath $I(f^1)$ and $I(f^2)$ which has to be accounted for when disentangling the two.

The Ce*M*In$_5$ data in Fig. 1 look very much alike. Only the Co data exhibit an extra hump at about 923 eV binding energy which is due to some intensity from the Co2*s* emission. We now compare qualitatively the ratio of the $I(f^2)/I(f^1)$ intensities for the Ce3d$_{5/2}$ emission: the ratio increases systematically from top to bottom,

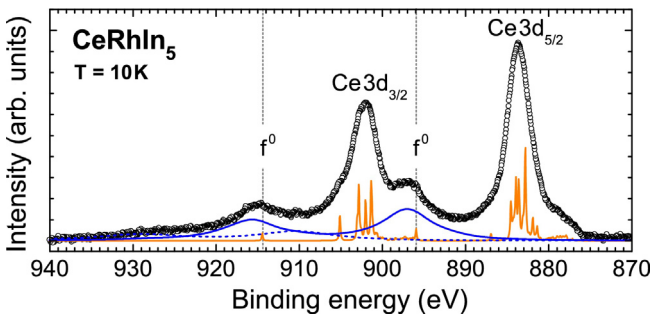

Fig. 3. Ce3*d* core level emission data of $CeRhIn_5$ after subtraction of the integral background. The blue lines (solid and dashed) represent the total 1st and 2nd order plasmon intensities which were obtained by fitting each emission line of the multiplet structure (orange, times 0.1) with a line shape consisting of a main emission line plus a 1st and 2nd plasmon contribution at equidistant energies. The vertical gray lines indicate the single emission line of $I(f^0)$.

i.e. from the Ce*M*In_5 family to $CePd_3$. However the intensity ratio $I(f^0)/I(f^1)$ seemingly does not have the same systematic when comparing the intensities at the $I(f^0)$ position at 915 eV. For the Ce*M*In_5 $I(f^0)/I(f^1)$ seems larger than for $CeRu_2Si_2$. This is puzzling since increasing hybridization should lead to an increase of both $I(f^2)/I(f^1)$ and $I(f^0)/I(f^1)$.

This puzzle is quickly solved when looking at the In3*p* emission spectra of the Ce*M*In_5 compounds at the top of Fig. 2. Strong and relatively sharp intensities in addition to the main In3$p_{1/2}$ and In3$p_{3/2}$ emission lines are visible at about 13–14 eV higher binding energies, respectively, and they are identified as plasmonic excitations. This is about the energy distance of the $I(f^0)$ and $I(f^1)$ spectral weights in the Ce3*d* core level spectra, meaning the $I(f^0)$ intensities in the Ce*M*In_5 data are superimposed by plasmons as already pointed out by the authors of Refs. [33,36], leading to the misleading impression that the $I(f^0)$ spectral weight in the 115 compounds is larger than in $CeRu_2Si_2$.

The data analysis comprises (1) the background correction, (2) the plasmon correction, (3) the assignment of spectral weights, and (4) the conversion of final state spectral weights $I(f^n)$ into initial state contributions w_n with the CI calculation. Step (1) is straightforward and an integrated background as marked by the black lines in Fig. 1 is subtracted from the data before further analysis. In the presence of strong plasmons the steps (2)–(4) have to be performed in one go by using line shapes for the multiplet excitations that consist of the main emission plus a first and second order plasmon.

The plasmon contributions to the line shapes are determined from fits to the core hole emissions spectra (after background correction) that are not affected by the configuration interaction. These spectra and line-shape fits are shown in Fig. 2 for all compounds. The lines are broadened by a Gaussian and Lorentzian function to account for instrumental resolution and lifetime broadening. In addition a Mahan function is used to account for the asymmetry of the line shapes. Then a single and double plasmon excitation is attached to each multiplet line. The plasmon excitations in $CeRu_2Si_2$, $CeRh_3B_2$, and $CePd_3$ are much broader than in the Ce*M*In_5 compounds and appear at larger energy distances from the main emission line. Nevertheless the same procedure was used for all compounds. The resulting plasmon parameters are listed in the Appendix B in Table 2.

Having determined the plasmon energies, line widths and intensity ratios, the combined fm-CI is applied to the background-corrected Ce3*d* data. The plasmon contributions in the Ce3*d* emission data of the Ce*M*In_5 resulting from such a fit are shown exemplary for $CeRhIn_5$ in Fig. 3 and for the other compounds in Fig. 1 (see solid (1st) and dashed (2nd) blue lines). Finally, Fig. 4 shows the background- and plasmon-corrected data (open circles).

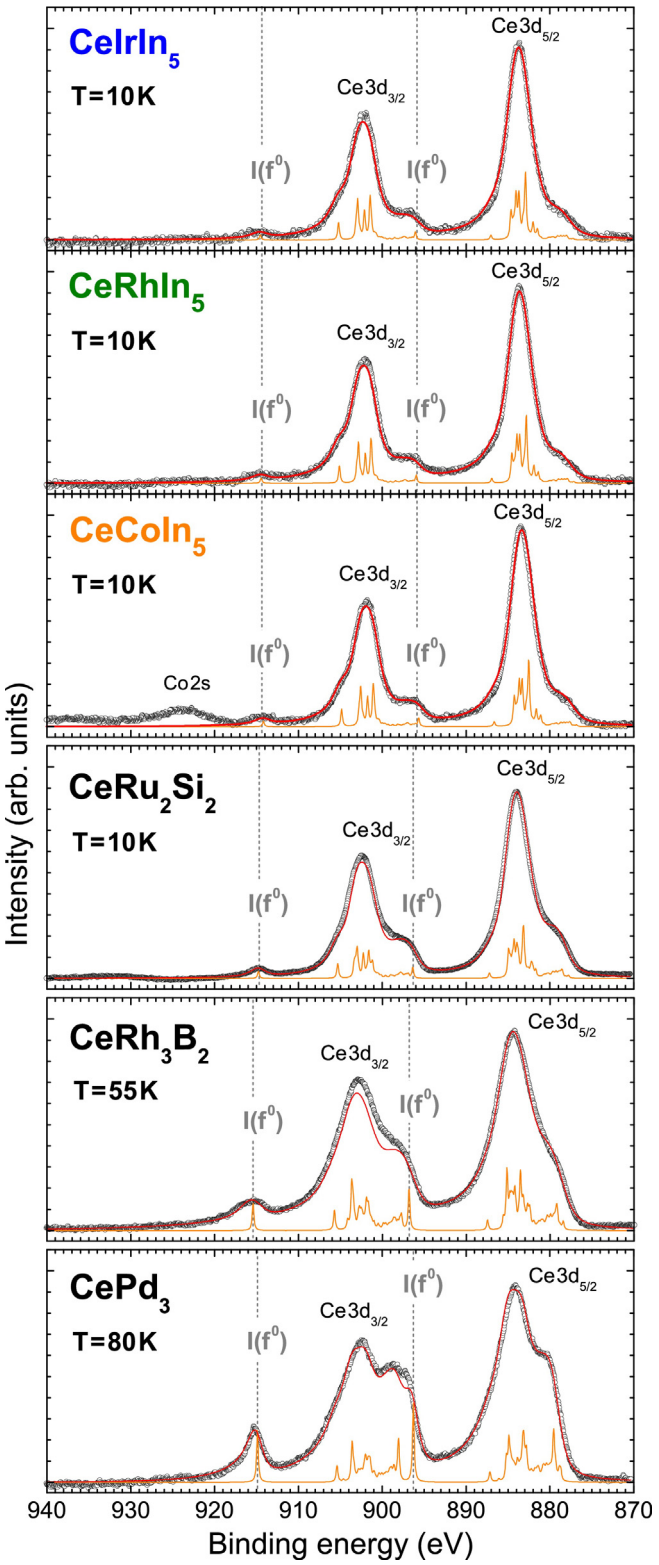

Fig. 4. Ce3*d* emission data after background and plasmon subtraction (black circles). The red lines are the result of the fm-CI calculation (see text), the orange lines resemble the corresponding multiplet structures times 0.1. The vertical dotted lines indicate the single emission line of $I(f^0)$. (For interpretation of the references to color in this figure legend, the reader is referred to the web version of this article.)

Now the ratios $I(f^0)/I(f^1)$ and $I(f^2)/I(f^1)$ are smallest for the 115 compounds. They increase to $CeRu_2Si_2$ and are largest for $CePd_3$. The red lines are the result of the fm-CI simulation. The resulting fit parameters and spectral weights are listed in Table 1. The complete set

Table 1
Top: Optimized configuration interaction parameters (U_{ff}, U_{fc}, $V_{\rm eff}$, ε_f) in eV and resulting f^n contributions w_0, w_1, and w_2 in the ground state in %. The total f electron count is given by $n_f = w_1 + 2w_2$.

		$CePd_3$	$CeRh_3B_2$	$CeRu_2Si_2$	$CeCoIn_5$	$CeRhIn_5$	$CeIrIn_5$
U_{ff}	[eV]	11.4	10.2	9.2	8.5	8.5	8.5
U_{fc}	[eV]	11.6	10.9	9.9	9.9	9.9	9.9
$V_{\rm eff}$	[eV]	0.36	0.31	0.25	0.20	0.20	0.20
ε_f	[eV]	1.3	2.0	2.6	2.4	2.4	2.4
w_0	[%]	24.0 (±3.0)	13.5 (±3.0)	6.8 (±1.2)	5.0 (±1.5)	4.7 (±1.5)	4.7 (±1.5)
w_1	[%]	74.0 (±3.0)	83.7 (±3.0)	90.3 (±1.2)	93.0 (±1.5)	93.3 (±1.5)	93.3 (±1.5)
w_2	[%]	2.0 (±0.5)	2.6 (±0.5)	2.9 (±0.5)	2.0 (±0.5)	2.0 (±0.5)	2.0 (±0.5)

Table 2
Line shape parameters of the Ce3d emission lines; Gaussian FWHM_G, Lorentzian FWHM_L, and the Mahan broadening with asymmetry α_M and cut-off γ_M, plus the plasmon energy ΔE^{Pl} and width of the plasmon excitation FWHM_L^{Pl}.

		$CePd_3$	$CeRh_3B_2$	$CeRu_2Si_2$	$CeCoIn_5$	$CeRhIn_5$	$CeIrIn_5$
FWHM_G	[eV]	1.1	2.0[a]	1.1	1.1	1.1	1.1
FWHM_L	[eV]	1.14	1.36	1.44	1.36	1.36	1.3
α_M		0.40	0.2	0.1	0.14	0.14	0.14
γ_M	[eV]	5	15	6	6	8	6
ΔE^{Pl}	[eV]	29	29	22	13.2	13.4	13.4
FWHM_L^{Pl}	[eV]	14	18	10[b]	3.4	3.8	3.8

[a] Value estimated from Fermi fit of the wide scan, since broadening appears larger than for the Au film.
[b] Plus Mahan type broadening of $\alpha_M = 0.8$ and $\gamma_M = 8$ eV.

of lineshape parameters is given in Table 2. The orange lines indicate the underlying multiplet structures. Note, $I(f^0)$ consists of only one emission line so that it remains visible even when the intensity is rather weak (see vertical gray lines in Fig. 4 marking the sharp peaks in the multiplet structure at ≈915 and ≈896 eV).

We also show PFY-XAS data where the $L_{\alpha 1}$ decay process $3d_{5/2} \rightarrow 2p_{3/2}$ after the L_3 absorption $2p \rightarrow 5d$ is measured (see Fig. 5(a)) in order to confirm our HAXPES result of a minor and very similar cf-hybridization in the CeMIn$_5$ compounds. Also here we find that at 20 K the spectra of all three compounds are identical within the accuracy of the measurement. It is actually next to impossible to spot the $I(f^0)$ spectral weight also when comparing the data at 20 K with data taken at 200 K (not shown). Band structure calculations of the empty 5d-DOS neglecting core hole effects (see Appendix C) show that the structures at 5733 and 5746 eV are due to band structure (see dashed and solid black lines in Fig. 5(a)). However, comparing the PFY-XAS data of the Ce115s with the PFY-XAS data of the more strongly hybridized CeT_2Al$_{10}$ compounds quickly shows where the $I(f^0)$ spectral weight should be. $CeFe_2Al_{10}$ is known to be more strongly intermediate-valent than the T = Ru and Os samples [53] and there is indeed a large difference in the spectra. The strongest absorption line at 5726 eV is strongly reduced while the intensity at 5737 eV is enhanced, i.e. the latter must be the $I(f^0)$ spectral weight. Also here the band structure calculations reproduce the overall features of the multiple scattering process and the similarity of the 5d-DOS of $CeFe_2Al_{10}$ (green line) and $CeRu_2Al_{10}$ (orange line) in Fig. 5(c) confirms that the difference in the data must indeed be due to the difference in $I(f^n)$ spectral weights. The respective central energy positions of the $I(f^n)$ are marked in Fig. 5(a).

In Fig. 5(b) we show a consistency fit to the PFY data of CeMIn$_5$. Applying a CI calculation using the same initial state Hamiltonian as for HAXPES yields also good results for the PFY-XAS data when using identical lineshapes for each $I(f^n)$, consisting of three Gaussians, a tanh-type step function with inflection point nearby the maximum of the respective $I(f^n)$ absorption, and an additional Gaussian for mimicking the multiple scattering peak. This choice of lineshape has actual similarities with the empty 5d-DOS in Fig. 5(a). Here the weighted, averaged energy distributions of the multiplet

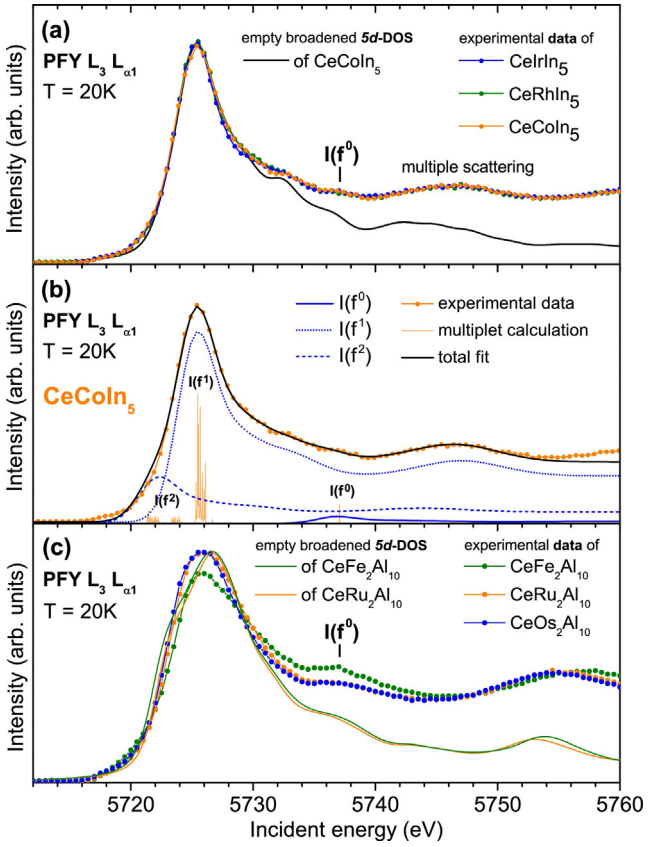

Fig. 5. (a) L-edge PFY-XAS spectra of CeMIn$_5$ normalized to the energy region beyond 5742 eV. The black lines resemble Wien2k calculations of the unoccupied 5d-DOS for $CeCoIn_5$. (b) Simulation of $CeCoIn_5$ data with identical line shapes for each $I(f^n)$ based on a CI model with parameters as for HAXPES, only U_{fc} was adjusted (see text). The line shapes are approximated by Gaussians and a step function (see text). The orange lines are the underlying multiplet structure of each $I(f^n)$ (see text). (c) L-edge PFY-XAS data of CeT_2Al$_{10}$ with T = Fe, Ru, and Os plus 5d-DOS from Wien2k calculations for $CeFe_2Al_{10}$ and $CeRu_2Al_{10}$. (For interpretation of the references to color in this figure legend, the reader is referred to the web version of this article.)

states define the energy separations of the respective $I(f^n)$. The red line resembles the total fit. Here only the CI parameter U_{fc} has been adjusted from 9.9 as for HAXPES to 9 eV for PFY-XAS in order to match the energy position of $I(f^0)$. Please note that the same adjustment is necessary for CeT_2Al_{10} where HAXPES yields an U_{fc} of 10 eV [53] while the present PFY-XAS data require 9 eV. The reason is most likely the screening of the 2*p* hole in the XAS final state by the additional 5*d* electron.

3. Results and discussion

The present results shall be briefly compared with some of the data available in literature before discussing the systematic of the resulting CI parameters in Table 1. There are several electron spectroscopy measurements of the valence of $CePd_3$. To name some, TFY L_3-edge absorption yields values of about ≈3.15 [43,44] and PES data by Fuggle et al. [21] and Kotani et al. [23] yield an f^0 contribution of w_0= 10% and an *f*-occupation of n_f= 0.86, respectively. The last two works take final state effects into account. We find a stronger deviation from an integer *f*-occupation which might be due to the fact that the before mentioned PES data suffer from surface effects which result in an *f* occupation closer to integer [25].

Also in $CeRh_3B_2$ the presence of an important amount of f^0 in the *L*-edge XAS data was reported [48] and an *f* occupation of n_f= 0.85 was given from the quantitative analysis of 3*d* core level PES data by Fujimori et al. [49] The PES value is close to what we obtain from the bulk-sensitive data and we can only speculate why we find a slightly *smaller* deviation from integer valence in the bulk-sensitive data. Here surface effects are no explanation since they rather increase the *f*-occupation [25]. However, our total fm-CI fit to the $CeRh_3B_2$ data is not that perfect and this might be due to the giant crystal-electric field (CEF) in this compound [54]. In contrast to Fujimori et al. [49], we used a single crystal for the HAXPES experiment and possible polarization dependencies due to CEF effects as recently reported [55] are not part of our calculation. Hence there is room for some error.

For $CeRu_2Si_2$ some bulk-sensitive HAXPES data, analyzed with an AIM are available [56]. Here the valence band continuum was divided into N= 21 discrete levels and the spectral weights were assigned empirically. The f^0 occupation is almost the same as from our analysis, but the CI-parameters differ and the empirical assignment of $I(f^2)$ seems to lead to an overestimation of the latter (n_f= 0.987, w_0= 5%, and w_2= 4.7% according to Yano et al. [56]).

The values in Table 1 show the largest values for U_{ff} and U_{fc} for the most strongly hybridized compounds $CePd_3$. For the more weakly hybridized compounds the fits were less sensitive to U_{fc} so that it was kept at a constant value of 9.9 eV. The effective hybridization V_{eff} is clearly largest for intermediate valent $CePd_3$ and smallest for the Ce*M*In_5 compounds while their effective *f* electron binding energy ε_f is comparable to that $CeRu_2Si_2$. The resulting f^n contributions in the ground state wave function are also given in Table 1 and we can clearly state that the Ce*M*In_5 compounds have the smallest f^0 contribution in the ground state, even less than $CeRu_2Si_2$. Interestingly, the f^2 contribution in the ground state (w_2) is almost the same (about 2–3%) for *all* compounds, from strongly intermediate valent $CePd_3$ to the much less hybridized Ce*M*In_5, emphasizing the importance of final state effects. In the final state, f^1 and f^2 are close in energy and therefore strongly entangled. As a result, the spectral weights $I(f^2)$ may be fairly strong in HAXPES as well as PFY-XAS.

Let us now look at the role of the transition metal elements for the ground state of the Ce*M*In_5 compounds. Within the accuracy of the present HAXPES and PFY-XAS data, the 4*f* shell occupation is essentially the same. This is to be contrasted with, e.g., the CeM_2 family with *M*= Co, Rh, and Ir where the *cf*-hybridization and *f* electron delocalization increases with increasing delocalization of the transition metal *d* electrons, i.e. with increasing atomic number [57,58]. This different behavior for the Ce115s implies that the transition metals should rather be treated as a *perturbation* which is plausible when looking at the crystal structure. The Ce*M*In_5 structure consists of distorted $CeIn_3$ blocks with intercalated MIn_2 layers [59,11]. Nearest and next-nearest neighbors of Ce are the in- and out-of-plane In atoms, whereas the transition metal ions are only the third nearest neighbors. Note that the parent compound $CeIn_3$ orders antiferromagnetically at 10 K and exhibits pressure induced superconductivity [60].

The small impact of the transition metal ions on the 4*f* density of states in the vicinity of the Fermi energy is also supported by band structure calculations by Maehira et al. [61] who have instead inferred that the differences in the ground state could be caused by the transition metal induced changes of the 4*f* crystal-electric field. This was then indeed verified experimentally for $CeRh_{1-x}Ir_xIn_5$ and $CeCoIn_5$[62]; the more elongated *f* ground state orbitals favor the superconducting ground state. These findings agree well with first-principle dynamical mean field theory calculations by Shim et al. [63] which postulated for $CeIrIn_5$ that the out-of-plane hybridization with the so-called In(2) is the most important one. Hence, it is not the absolute strength of the *cf*-hybridization (and occupation) that changes among the Ce*M*In_5 compounds, it rather seems to be the *efficiency* of hybridization that depends on the orbital anisotropy. Looking beyond the idea of isotropic hybridization may then rationalize the seemingly contradicting results of identical *f*-occupations but different Fermi surfaces in superconducting $CeIrIn_5$ and $CeCoIn_5$ and magnetically ordered $CeRhIn_5$[13–17,20,18,19].

4. Summary

The *f*-occupation of the Ce*M*In_5 family has been investigated with bulk-sensitive HAXPES and PFY-XAS and compared with spectra of cerium compounds of different hybridization strengths. The PFY-XAS data show that the *f*-occupation of the Ce*M*In_5 compounds is identical within the accuracy of the present experiments. A detailed analysis of the HAXPES data, which includes a quantitative plasmon correction, shows further that the effective hybridization V_{eff} and also the amount of f^0 in the ground state in the Ce*M*In_5 is even smaller than in the non-magnetically ordering compound $CeRu_2Si_2$.

Acknowledgements

For M.S., F.S. and A.S. this work was supported by DFG through project 600575. We thank S. Wirth for fruitful discussions and reading the manuscript. The PFY experiment was performed under the approvals with Japan Synchrotron Radiation Research Institute (Proposal No. 2011A4254, 2012A4252, 2012B4251) and National Synchrotron Radiation Research Center, Taiwan (2011-2-053, 2012-3-078). Work at Los Alamos was performed under the auspices of the U.S. Department of Energy, Office of Basic Energy Sciences, Division of Materials Sciences and Engineering.

Appendix A. Experimental set-ups

The HAXPES spectra of the Ce 3*d* emission were taken at the Taiwan beamline BL12XU at SPring-8 with an incident energy of 6.5 keV and horizontally polarized light. An MB Scientific A1-HE analyzer at an angle of 90° to the incident beam in the vertical (horizontal for $CeRh_3B_2$) plane gives an overall instrumental resolution of ≈1 eV at the Ce 3*d* emission using a pass energy of 200 eV and fully opened slits (S3.2). The Fermi energy and instrumental

resolution was obtained by measuring the valence band spectra of silver or gold thin films. Clean sample surfaces were obtained by cleaving *in situ* under ultra high vacuum of the order of 10^{-9} mbar and the reproducibility of successively taken scans showed the absence of aging effects. Only $CeRh_3B_2$ showed one additional line at C1*s* energy, indicating some graphite on the surface, which may also explain the larger broadening in this compound. For the other samples, scans over a wide energy range, from the Fermi energy to 1 keV binding energy, verified the absence of impurities.

The PFY-XAS experiments were performed at the inelastic scattering beamline with a Johann-type set-up at the synchrotron SPring-8 in Japan (BL12XU beamline). The undulator beamline uses a cryogenically-cooled double crystal monochromator to obtain a monochromatic beam. The $3d_{5/2} \rightarrow 2p_{3/2}$ de-excitation of 4800 eV at the Ce L_3 absorption edge was measured as function of the incident energy. The emission line was analyzed with a spherically bent Si(400) analyzer crystal (radius 1 m). The analyzed photons were detected in Si solid state detectors (Amptech) with an overall energy resolutions of $\approx$ 1.5 eV. The intensities of the measured spectra were normalized with a monitor just before the sample. The beam size was $120(h) \times 80(v)\,\mu m^2$. The flight path was filled with He to reduce air scattering. The closed-circuit He cryostat reached a base temperature of 20 K.

The Ce*M*In_5 single crystals were grown with the flux growth method, the $CeRu_2Si_2$ and the $CeRh_3B_2$ single crystals by the Czochralski technique. The $CePd_3$ polycrystalline sample was made by arc-melting the constituents on a water-cooled Cu hearth under a UHP Argon atmosphere. Polycrystalline samples of CeT_2Al_{10} were prepared by arc-melting the constituents amounting of pure elements under Argon atmosphere and annealing at 850 °C for one weak.

Appendix B. Simulation

The data have been analyzed with the combined fm-CI model as described in detail in Ref. [53]. For the fm-CI simulations the XTLS 9.0 code by Tanaka was used [64] and the atomic input parameters for the intra-atomic 4*f*-4*f* and 3*d*-4*f* Coulomb and exchange interactions and the 3*d* and 4*f* spin-orbit coupling were calculated with Cowan's atomic structure code [65]. Reduction factors of ≈40% and ≈20% for the atomic Hartree–Fock values for the 4*f*–4*f* and 3*d*–4*f* Coulomb interaction were used [53]. The hybridization between the *f* and conduction electrons is described by the Coulomb exchange interaction between the *f* electrons (U_{ff}) and between the *f* electrons and 3*d* core hole (U_{fc}), the effective *f*-electron binding energy ε_f (i.e. the mean energy difference between the f^0 and $f^1\underline{L}$ in the initial state) and the isotropic hybridization V_{eff}.

Plasmons appear at well-defined energies at higher binding energies so that the full multiplet calculations allows the pinning of a plasmon and its multiples to each emission line with the same energy distance, line width and shape. The line shape parameters for life time broadening (Lorentzian & Mahan) and the energies and relative intensities of 1st and 2nd plasmons were determined from fitting the core level spectra of another element in the sample which is not affected by the CI [53]). We used In3*p* for the Ce*M*In_5 compounds, Pd3*p* for $CePd_3$, Rh3*d* for $CeRh_3B_2$, Ru3*d* for $CeRu_2Si_2$. The line shape parameters which were used in the data analysis are listed in Table 2.

Appendix C. Band structure

The electronic structure calculations have been performed using the WIEN2k program package [66]. The generalized gradient approximation has been used for the exchange-correlation potential [67]. The Ce 4*f* states have been treated as *open core*. This assures the Ce ions are trivalent and a direct influence on the 5*d* density of states (5*d*-DOS) is avoided. The calculations were converged below a charge distance of 10^{-5} on a $13\times13\times10$ mesh of *k* points with $RK_{max} = 8.0$. The DOS has been calculated on a $26\times26\times10$ mesh. Core hole effects were not taken into account *in order to keep the calculation simple*. The calculations are based on the actual 300 K structure parameters of the respective compounds [59,68–70].

References

[1] P. Gegenwart, Q. Si, F. Steglich, Nat. Phys. 4 (2008) 186.
[2] H. Hegger, C. Petrovic, E.G. Moshopoulou, M.F. Hundley, J.L. Sarrao, Z. Fisk, J.D. Thompson, Phys. Rev. Lett. 84 (2000) 4986.
[3] V.S. Zapf, E.J. Freeman, E.D. Bauer, J. Petricka, C. Sirvent, N.A. Frederick, R.P. Dickey, M.B. Maple, Phys. Rev. B 65 (2001) 014506.
[4] C. Petrovic, P.G. Pagliuso, M.F. Hundley, R. Movshovich, J.L. Sarrao, J.D. Thompson, Z. Fisk, P. Monthoux, J. Phys.: Condens. Matter 13 (2001) L337.
[5] C. Petrovic, R. Movshovich, M. Jaime, P.G. Pagliuso, M.F. Hundley, J.L. Sarrao, Z. Fisk, J.D. Thompson, Europhys. Lett. 53 (2001) 354.
[6] P.G. Pagliuso, C. Petrovic, R. Movshovich, D. Hall, M.F. Hundley, J.L. Sarrao, J.D. Thompson, Z. Fisk, Phys. Rev. B 64 (2001) 100503.
[7] P.G. Pagliuso, R. Movshovich, A.D. Bianchi, M. Nicklas, N.O. Moreno, J.D. Thompson, M.F. Hundley, J.L. Sarrao, Z. Fisk, Phys. B 312–313 (2002) 129.
[8] A. Llobet, A.D. Christianson, W. Bao, J.S. Gardner, I.P. Swainson, J.W. Lynn, J.-M. Mignot, K. Prokes, P.G. Pagliuso, N.O. Moreno, J.L. Sarrao, J.D. Thompson, A.H. Lacerda, Phys. Rev. Lett. 95 (2005) 217002.
[9] T. Park, F. Ronning, H.Q. Yuan, M.B. Salamon, R. Movshovich, J.L. Sarrao, J.D. Thompson, Nature 65 (2006) 440.
[10] S. Ohira-Kawamura, H. Shishido, A. Yoshida, R. Okazaki, H. Kawano-Furukawa, T. Shibauchi, H. Harima, Y. Matsuda, Phys. Rev. B 76 (2007) 132507.
[11] J.D. Thompson, Z. Fisk, J. Phys. Soc. Japan 81 (2012) 011002, and references therein.
[12] P. Aynajian, E.H. da Silva Neto, A. Gyenis, R.E. Baumbach, J.D. Thompson, Z. Fisk, E.D. Bauer, A. Yazdani, Nature 486 (2012) 201.
[13] Y. Haga, Y. Inada, H. Harima, K. Oikawa, M. Murakawa, H. Nakawaki, Y. Tokiwa, D. Aoki, H. Shishido, S. Ikeda, N. Watanabe, Y. Ōnuki, Phys. Rev. B 63 (2001) 060503.
[14] S.-I. Fujimori, T. Okane, J. Okamoto, K. Mamiya, Y. Muramatsu, A. Fujimori, H. Harima, D. Aoki, S. Ikeda, H. Shishido, Y. Tokiwa, Y. Haga, Y. Onuki, Phys. Rev. B 67 (2003) 144507.
[15] N. Harrison, U. Alver, R.G. Goodrich, I. Vekhter, J.L. Sarrao, P.G. Pagliuso, N.O. Moreno, L. Balicas, Z. Fisk, D. Hall, R.T. Macaluso, J.Y. Chan, Phys. Rev. Lett. 93 (2004) 186405.
[16] H. Shishido, R. Settai, H. Harima, Y. Onuki, J. Phys. Soc. Japan 74 (2005) 1103.
[17] R. Settai, T. Takeuchi, Y. Onuki, J. Phys. Soc. Japan 76 (2007) 051003.
[18] H. Shishido, R. Settai, T. Kawai, H. Harima, Y. Onuki, J. Magn. Magn. Mater. 310 (2007) 303.
[19] S.K. Goh, J. Paglione, M. Sutherland, E.C.T. O'Farrell, C. Bergemann, T.A. Sayles, M.B. Maple, Phys. Rev. Lett. 101 (2008) 056402.
[20] M.P. Allen, F. Massee, D.K. Morr, J. Van Dyke, A.W. Rost, A.P. Mackenzie, C. Petrovic, J.C. Davis, Nat. Phys. 9 (2013) 468.
[21] J.C. Fuggle, F.U. Hillebrecht, Z. Zolnierek, R. Lässer, C. Freiburg, O. Gunnarsson, K. Schönhammer, Phys. Rev. B 27 (1983) 7330.
[22] O. Gunnarsson, K. Schönhammer, Phys. Rev. B 28 (1983) 4315.
[23] A. Kotani, T. Jo, J. Parlebas, Adv. Phys. 37 (1988) 37.
[24] O. Gunnarsson, K. Schnhammer, J. Allen, K. Karlsson, O. Jepsen, J. Electron Spectrosc. 117–118 (2001) 1.
[25] C. Laubschat, E. Weschke, C. Holtz, M. Domke, O. Strebel, G. Kaindl, Phys. Rev. Lett. 65 (1990) 1639.
[26] K. Hämälä inen, D.P. Siddons, J.B. Hastings, L.E. Berman, Phys. Rev. Lett. 67 (1991) 2850.
[27] A. Kotani, S. Shin, Rev. Mod. Phys. 73 (2001) 203.
[28] C. Dallera, M. Grioni, A. Shukla, G. Vankó, J.L. Sarrao, J.P. Rueff, D.L. Cox, Phys. Rev. Lett. 88 (2002) 196403.
[29] J.-P. Rueff, A. Shukla, Rev. Mod. Phys. 82 (2010) 847.
[30] Y. Zekko, Y. Yamamoto, H. Yamaoka, F. Tajima, T. Nishioka, F. Strigari, A. Severing, J.-F. Lin, N. Hiraoka, H. Ishii, K.-D. Tsuei, J. Mizuki, Phys. Rev. B 89 (2014) 125108.
[31] M. Daniel, S.-W. Han, C.H. Booth, A.L. Cornelius, P.G. Pagliuso, J.L. Sarrao, J.D. Thompson, Phys. Rev. B 71 (2005) 054417.
[32] S.-I. Fujimori, A. Fujimori, K. Shimada, T. Narimura, K. Kobayashi, H. Namatame, M. Taniguchi, H. Harima, H. Shishido, S. Ikeda, D. Aoki, Y. Tokiwa, Y. Haga, Y. Ōnuki, Phys. Rev. B 73 (2006) 224517.
[33] M. Gamża, A. Ślebarski, J. Deniszczyk, J. Phys.: Condens. Matter 20 (2008) 115202.
[34] T. Willers, Z. Hu, N. Hollmann, P.O. Körner, J. Gegner, T. Burnus, H. Fujiwara, A. Tanaka, D. Schmitz, H.H. Hsieh, H.-J. Lin, C.T. Chen, E.D. Bauer, J.L. Sarrao, E. Goremychkin, M. Koza, L.H. Tjeng, A. Severing, Phys. Rev. B 81 (2010) 195114.
[35] C.H. Booth, T. Durakiewicz, C. Capan, D. Hurt, A.D. Bianchi, J.J. Joyce, Z. Fisk, Phys. Rev. B 83 (2011) 235117.
[36] U. Treske, M. Khoshkhoo, F. Roth, M. Knupfer, E. Bauer, J. Sarrao, B. Büchner, A. Koitzsch, J. Phys.: Condens. Matter 26 (2014) 205601.

[37] L. Howald, E. Stilp, P. Dalmas de Reotier, A. Yaouanc, S. Raymond, C. Piamonteze, G. Lapertot, C. Baines, H. Keller, Sci. Rep. 5 (2015) 12528.
[38] A. Kotani, H. Mizuta, T. Jo, Solid State Commun. 53 (1985) 805.
[39] T. Jo, A. Kotani, Solid State Commun. 54 (1985) 451.
[40] C.F. Hague, J.-M. Mariot, R. Delaunay, J.-J. Gallet, L. Journel, J.-P. Rueff, J. Electron Spectrosc. 136 (2004) 179.
[41] A. Kotani, K.O. Kvashnina, S.M. Butorin, P. Glatzel, J. Electron Spectrosc. 184 (2011) 210.
[42] H. Schneider, D. Wohlleben, Z. Phys. B: Condens. Matter 44 (1981) 193.
[43] A. Bianconi, M. Campagna, S. Stizza, I. Davoli, Phys. Rev. B 24 (1981) 6139.
[44] M. Croft, R. Neifeld, C.U. Segre, S. Raaen, R.D. Parks, Phys. Rev. B 30 (1984) 4164.
[45] A.P. Murani, A. Severing, W.G. Marshall, Phys. Rev. B 53 (1996) 2641.
[46] J.M. Fanelli, V.R. amd Lawrence, E.A. Goremychkin, R. Osborn, E.D. Bauer, K.J. McClellan, J.D. Thompson, C.H. Booth, A.D. Christianson, P.S. Riseborough, J. Phys.: Condens. Matter 26 (2014) 225602.
[47] S.K. Dhar, S.K. Malik, R. Vijayaraghavan, J. Phys. C: Solid State 14 (1981) L321.
[48] E.V. Sampathkumaran, G. Kaindl, C. Laubschat, W. Krone, G. Wortmann, Phys. Rev. B 31 (1985) 3185.
[49] A. Fujimori, T. Takahashi, A. Okabe, M. Kasaya, T. Kasuya, Phys. Rev. B 41 (1990) 6783.
[50] J. Flouquet, Prog. Low Temp. Phys. 15 (2005) 139.
[51] H. Aoki, N. Kimura, T. Terashima, J. Phys. Soc. Japan 83 (2014) 072001.
[52] J.-M. Imer, E. Wuilloud, Z. Phys. B: Condens. Matter 66 (1987) 153.
[53] F. Strigari, M. Sundermann, Y. Muro, K. Yutani, T. Takabatake, K.-D. Tsuei, Y. Liao, A. Tanaka, P. Thalmeier, M. Haverkort, L. Tjeng, A. Severing, J. Electron Spectrosc. 199 (2015) 56.
[54] F. Givord, J.-X. Boucherle, A. Murani, R. Bewley, R.-M. Galra, P. Lejay, J. Phys.: Condens. Matter 19 (2007) 506210.
[55] T. Mori, S. Kitayama, Y. Kana, S. Naimen, H. Fujiwara, A. Higashiya, K. Tamasaku, A. Tanaka, K. Terashima, S. Imada, A. Yasu, Y. Saitoh, K. Yamagami, K. Yano, T. Matsumoto, T. Kiss, M. Yabashi, T. Ishikawa, S. Suga, Y. Ånuki, T. Ebihara, A. Sekiyama, J. Phys. Soc. Japan 83 (2014) 123702.
[56] M. Yano, A. Sekiyama, H. Fujiwara, Y. Amano, S. Imada, T. Muro, M. Yabashi, K. Tamasaku, A. Higashiya, T. Ishikawa, Y. Ōnuki, S. Suga, Phys. Rev. B 77 (2008) 035118.
[57] G. Chiaia, P. Vavassori, L. Duo, L.Q.M. Braicovich, I. Lindau, Surf. Sci 331–333 (1995) 1229.
[58] C. Laubschat, E. Weschke, M. Domke, C.T. Simmons, G. Kaindl, Surf. Sci. 269–270 (1992) 605.
[59] E.G. Moshopoulou, J.L. Sarrao, P.G. Pagliuso, N.O. Moreno, J.D. Thompson, Z. Fisk, R.M. Ibberson, Appl. Phys. A 74 (Suppl.) (2002) 895.
[60] N. Mathur, F.M. Grosche, S.R. Julian, L.R. Walker, D.M. Freye, R.K.W. Haselwimmer, G.G. Lonzarich, Nat. Phys. 394 (1998) 39.
[61] T. Maehira, T. Hotta, K. Ueda, A. Hasegawa, J. Phys. Soc. Japan 72 (2003) 854.
[62] T. Willers, F. Strigari, Z. Hu, V. Sessi, N.B. Brookes, E.D. Bauer, J.L. Sarrao, J.D. Thompson, A. Tanaka, S. Wirth, L.H. Tjeng, A. Severing, Proc. Natl. Acad. Sci. U. S. A. 112 (2015) 2384.
[63] J.H. Shim, K. Haule, G. Kotliar, Science 318 (2007) 1615.
[64] A. Tanaka, T. Jo, J. Phys. Soc. Japan 63 (1994) 2788.
[65] R.D. Cowan, The Theory of Atomic Structure and Spectra ed, University of California Press, Berkeley, 1981, ISBN:9780520038219.
[66] P. Blaha, K. Schwarz, G. Madsen, D. Kvasnicka, J. Luitz, in: K. Schwarz (Ed.), Wien2k, An Augmented Plane Wave + Local Orbitals Program for Calculating Crystal Properties, Tech. Universität Wien, Austria, 2001, ISBN:3-9501031-1-2.
[67] J.P. Perdew, K. Burke, M. Ernzerhof, Phys. Rev. Lett. 77 (1996) 3865.
[68] A.I. Tursina, S.N. Nesterenko, E.V. Murashova, I.V. Chernyshev, H. Noël, Y.D. Seropegin, Acta Crystallogr. E 61 (2005) i12.
[69] Y. Muro, K. Motoya, Y. Saiga, T. Takabatake, J. Phys. Soc. Japan 78 (2009) 083707.
[70] Y. Muro, J. Kajino, K. Umeo, K. Nishimoto, R. Tamura, T. Takabatake, Phys. Rev. B 81 (2010) 214401.